

Tunable Doping in Hydrogenated Single Layered Molybdenum Disulfide

Debora Pierucci, Hugo Henck, Zeineb Ben Aziza, Carl H. Naylor, Adrian Balan, Julien E. Rault, Mathieu G. Silly, Yannick J. Dappe, François Bertran, Patrick Le Fèvre, et al.

▶ **To cite this version:**

Debora Pierucci, Hugo Henck, Zeineb Ben Aziza, Carl H. Naylor, Adrian Balan, et al.. Tunable Doping in Hydrogenated Single Layered Molybdenum Disulfide. ACS Nano, 2017, 11, pp.1755 - 1761. 10.1021/acsnano.6b07661 . cea-01500564

HAL Id: cea-01500564

https://cea.hal.science/cea-01500564

Submitted on 3 Apr 2017

HAL is a multi-disciplinary open access archive for the deposit and dissemination of scientific research documents, whether they are published or not. The documents may come from teaching and research institutions in France or abroad, or from public or private research centers.

L'archive ouverte pluridisciplinaire **HAL**, est destinée au dépôt et à la diffusion de documents scientifiques de niveau recherche, publiés ou non, émanant des établissements d'enseignement et de recherche français ou étrangers, des laboratoires publics ou privés.

ACSNANO www.acsnano.org

ARTICLE

Tunable Doping in Hydrogenated Single Layered Molybdenum Disulfide

Debora Pierucci,[†] Hugo Henck,[†] Zeineb Ben Aziza,[†] Carl H. Naylor,[‡] Adrian Balan,[‡] Julien E. Rault,[§] Mathieu G. Silly,[§] Yannick J. Dappe,[∥] François Bertran,[§] Patrick Le Fèvre,[§] Fausto Sirotti,[§] A. T. Charlie Johnson,[‡] and Abdelkarim Ouerghi*[,†]

[†]Centre de Nanosciences et de Nanotechnologies, CNRS, Univ. Paris-Sud, Université Paris-Saclay, C2N – Marcoussis, F91460 Marcoussis, France

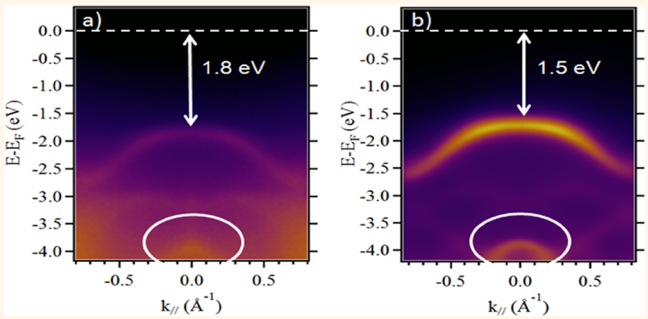
[‡]Department of Physics and Astronomy, University of Pennsylvania, 209S 33rd Street, Philadelphia, Pennsylvania 19104, United States

[§]Synchrotron-SOLEIL, Saint-Aubin, BP48, F91192 Gif sur Yvette Cedex, France

[∥]SPEC, CEA, CNRS, Université Paris-Saclay, CEA Saclay, F91191 Gif-sur-Yvette Cedex, France

Supporting Information

ABSTRACT: **Structural defects in the molybdenum disulfide (MoS_2) monolayer are widely known for strongly altering its properties. Therefore, a deep understanding of these structural defects and how they affect MoS_2 electronic properties is of fundamental importance. Here, we report on the incorporation of atomic hydrogen in monolayered MoS_2 to tune its structural defects. We demonstrate that the electronic properties of single layer MoS_2 can be tuned from the intrinsic electron (n) to hole (p) doping *via* controlled exposure to atomic hydrogen at room temperature. Moreover, this hydrogenation process represents a viable technique to completely saturate the sulfur vacancies present in the MoS_2 flakes. The successful incorporation of hydrogen in MoS_2 leads to the modification of the electronic properties as evidenced by high resolution X-ray photoemission spectroscopy and density functional theory calculations. Micro-Raman spectroscopy and angle resolved photoemission spectroscopy measurements show the high quality of the hydrogenated MoS_2 confirming the efficiency of our hydrogenation process. These results demonstrate that the MoS_2 hydrogenation could be a significant and efficient way to achieve tunable doping of transition metal dichalcogenides (TMD) materials with non-TMD elements.**



KEYWORDS: *n and p doped MoS_2, defects, atomic hydrogenation, doping, spectroscopy, electronic properties*

Following similar trend as graphene, the two-dimensional (2D) transition metal dichalcogenides (MX_2) have attracted much interest recently thanks to their versatile electronic and optical properties. However, unlike graphene that does not have a bandgap, they exhibit attractive properties such as indirect-to-direct bandgap crossover with decreasing number of atomic layers and strong photoresponses.[1−3] Moreover, 2D MX_2 materials have interesting electronic structure, *i.e.*, their tunable bandgap by varying the layer thickness and strain,[4,5] their edge-dependent semiconducting-to-metallic transitions,[6] in addition to the transformations between different S−Mo−S atoms stacking geometries (for instance, 2H to 1T phase of monolayer MoS_2[7]). In contrast to graphene where only small bandgap (few hundred meV) can be opened by strain and other methods,[8] large bandgap tunability can be obtained with 2D MX_2 where we can switch from a semiconducting (with a few eV bandgap) to a metallic form.[9] This large tunability allows broadening the applications of MX_2 in nanoelectronic devices.

Furthermore, the presence of defects can induce deep gap states responsible for the intrinsic doping of these materials.[10,11] For instance, in the case of MoS_2, sulfur monovacancies represent the defects with the lowest formation energy[12−14] and the most common generally present in MoS_2 flakes.[12] In particular, these sulfur vacancies (Sv) cause the presence of unsaturated electrons in the surrounding Mo atoms and act as electrons donors[15,16] responsible for the n-type doping of MoS_2.[17] It has already been demonstrated that the intercalation of oxygen,[18] nitrogen,[19] or niobium[20] can reduce the intrinsic

Received: November 14, 2016
Accepted: February 1, 2017
Published: February 1, 2017

ACS Publications © 2017 American Chemical Society

DOI: 10.1021/acsnano.6b07661
ACS Nano 2017, 11, 1755−1761

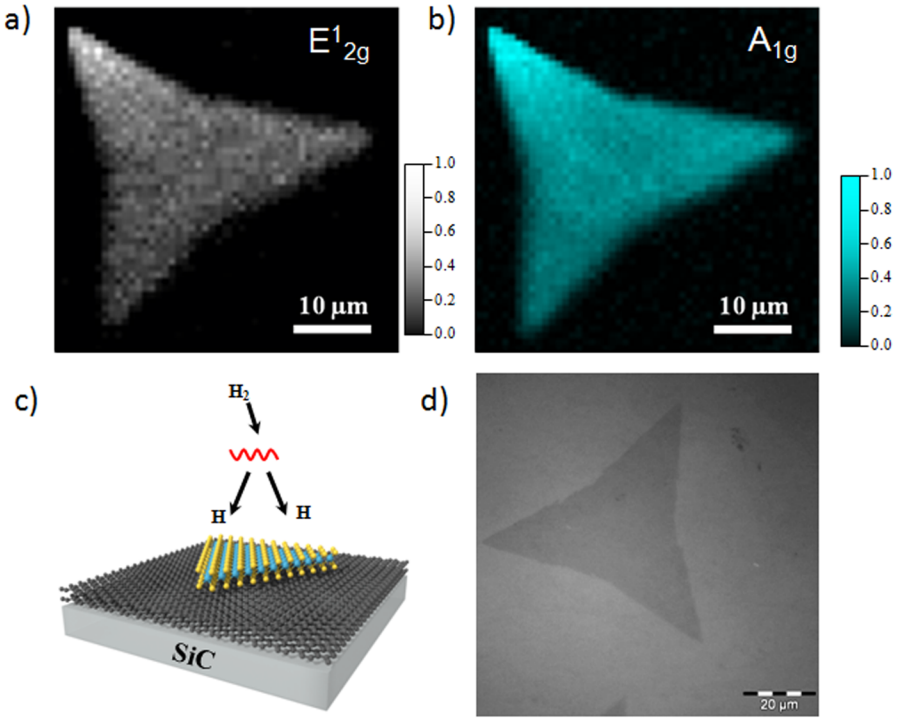


Figure 1. (a,b) Micro-Raman maps of E^1_{2g} and A_{1g} peaks of the MoS_2 on epitaxial graphene. (c) Schematic illustration of our current method for hydrogen-doped MoS_2. (d) Typical optical image of a hydrogenated MoS_2 flake on epitaxial graphene/SiC.

doping of MoS_2. Recent experiments using mainly Raman spectroscopy and high resolution X-ray photoemission spectroscopy (HR-XPS) demonstrated that the n doped MoS_2 can be tuned to p doped by N_2 plasma.[21] The introduction of dopants in MoS_2 lattice represents a potential route to achieve stable MoS_2 with different functionalities. Therefore, it is crucial to develop controllable techniques to make possible the tunability of MoS_2 properties without degrading the quality of MoS_2 flakes.

In this work we report an easy and effective chemical doping method by hydrogen atoms, already used as dopants for graphene[22,23] and we show that hydrogen represents an effective way to passivate sulfur vacancies. We study the electronic properties of the hydrogen-doped MoS_2, by exposing the sample to atomic hydrogen gas. HR-XPS studies reveal the n type doping of pristine single layer MoS_2 which is also confirmed by the measurement of the valence band maximum (VBM). We demonstrate that the atomic hydrogen doping can tune this intrinsic n doping until reaching p doped MoS_2. The analysis of the total density of states (LDOS) of the hydrogenated MoS_2 by first principle calculations using density functional theory (DFT) shows the presence of new gap states close to the VBM, confirming the p-type behavior of the hydrogenated MoS_2 on graphene. We also checked the quality of the hydrogenated MoS_2 using angle resolved photoemission spectroscopy (ARPES) measurements, which show sharp band structures. These results confirm the validity of the doping process without a degradation of the MoS_2 flakes.

RESULTS AND DISCUSSION

We used p-type graphene substrate obtained by hydrogenation of epitaxial graphene. This bilayer graphene/SiC(0001) presents several advantages. The graphene/SiC is conducting therefore particularly suited for XPS/ARPES measurements.[24] Also, the graphene presents a chemically inert surface due to the strong coupling of all its p_z atomic orbitals which are stabilized in a giant delocalized π bonding system.[25−27] This configuration inhibits the possibility of covalent addition and then the interaction with atomic hydrogen. Moreover, the prehydrogenation treatment of the graphene/SiC substrate,[28] ensures the saturation of the dangling bonds present at the SiC/buffer layer interface,[22] preventing the hydrogen intercalation in graphene during the MoS_2 treatment. Large (20−100 μm) MoS_2 flakes are grown by chemical vapor deposition (CVD) and then further deposited on the p doped bilayer graphene substrate using wet transfer process.[29] To further clean the surface and interface of the MoS_2/graphene heterostructure, we annealed the samples at T = 300 °C for 30 min in ultrahigh vacuum (UHV) ($P \approx 10^{-10}$ mbar).[30] More details about the growth and sample preparation are given in the Methods section.

After the transfer, the quality of the MoS_2 flakes was verified by Raman spectroscopy. The two Raman maps in Figure 1(a) and (b) show the intensity of the E^1_{2g} and A_{1g} Raman modes, respectively, of the MoS_2 on graphene layer. The two Raman peaks correspond to the in-plane vibrations (E^1_{2g}) and out of plane vibrations (A_{1g}) of Mo and S atoms in the MoS_2.[31] These maps reveal a large and uniform MoS_2 flake with only some variations of contrast in the whole flake. This uniformity of the peaks intensities indicates the good quality of our MoS_2 flakes. In order to investigate the effects of atomic hydrogen exposures to single layer MoS_2 on p doped bilayer graphene/SiC, the sample was exposed to several atomic hydrogen doses (~5×10^2 L, 5×10^3 L and 8×10^4 L, where 1 Langmuir (L) = 10^{-6} Torr × s). The molecular dihydrogen was cracked by a hot tungsten filament (1400 °C, approximately 5 cm from the sample), as illustrated in the schematic of Figure 1(c). Figure 1(d) shows an optical micrograph of a representative single layer flake on graphene/SiC after the hydrogenation process.

DOI: 10.1021/acsnano.6b07661
ACS Nano 2017, 11, 1755−1761

To examine the atomic composition as well as the chemical bonding environment of our samples, HR-XPS measurements at room temperature were carried out for pristine and hydrogen doped MoS_2. The spectra were collected in a surface sensitive condition at a photon energy at $h\nu$ = 340 eV (the photoelectrons were detected at 0° from the sample surface normal $\vec{n}$ and at 46° from the polarization vector $\vec{E}$). The C-1s spectrum corresponding to the underlayer p doped graphene is shown in Figure S1. The experimental data points are displayed as dots. The solid line is the envelope of fitted components. The pristine underlayer C 1s spectra consist of two components located at the binding energies of 282.5 and 284.3 eV. These components correspond to bulk SiC and bilayer graphene, respectively.[28] The shape and the position of the C 1s peak, arising from the graphene and the SiC underlayer, have not changed after the exposition to three hydrogen doses, with respect to the pristine one. This confirms that the hydrogen did not interact with the graphene/SiC underlayer. The evolution of the Mo 3d and S 2p peaks from the pristine MoS_2 through the three different hydrogen doses are shown in Figure 2(a) and (b), respectively. For the pristine

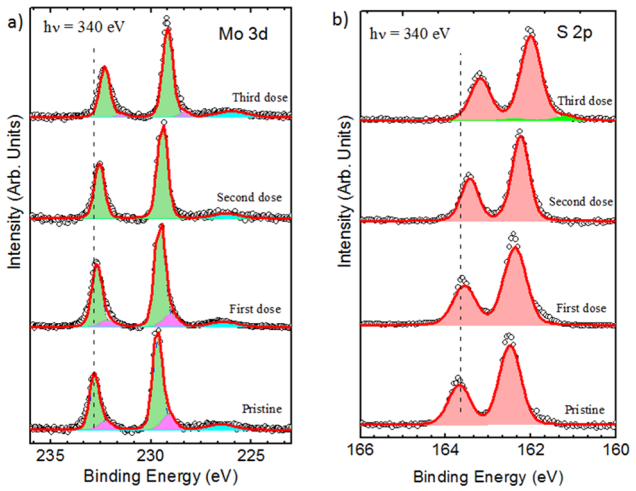


Figure 2. XPS measurement for MoS_2 at different doses of atomic hydrogen: (a) Mo-3d core level, (b) S-2p core level at $h\nu$ = 340 eV. The experimental data points are displayed as dots. The solid line is the envelope of fitted components.

MoS_2, the Mo 3d spectrum contains one main doublet component at binding energy (BE) Mo $3d_{5/2}$ = 229.7 eV ($3d_{5/2}$:$3d_{3/2}$ ratio of 0.66 and a spin−orbit splitting of 3.10 eV[32]) related to a Mo^{4+} in a sulfur environment[33] with a trigonal prismatic phase (1H-MoS_2). A smaller contribution visible at lower BE (∼−0.52 eV) with respect to this main doublet peaks is the signature of a defective/substoichiometric MoS_2 with Sv.[12,33] The weight of this component (between 15 and 18% of the whole Mo 3d spectrum) is not representative of a single MoS_2 flake due to the large X-ray beam size (∼100−150 μm diameter), but it gives information on the percentage of defective MoS_2 in the explored area. The additional peak at BE = 226.5 eV is due to the sulfur 2s peak. The S 2p spectrum of the pristine MoS_2 present only one main doublet at BE S $2p_{3/2}$ = 162. Five eV ($2p_{1/2}$:$2p_{3/2}$ ratio of 0.5 and a spin−orbit splitting of 1.19 eV[32]) as expected for divalent sulfide ions (S^{2-}) in 1H-MoS_2.[33,34] These BE values for the Mo 3d and S 2p indicate an intrinsic n-type doping of the MoS_2 flakes,[15] mostly induced by the Sv which act as an electron donating defects. No other components are present on the Mo 3d and S 2p spectra related to oxygen or carbon bonds[35−37] indicating that no contaminations are present on the sample and confirming the high quality of this heterostructure.

After the first exposure to atomic hydrogen, the core level peaks of Mo 3d and S 2p show a rigid shift of about 0.1 eV toward lower binding energies. The peaks related to Sv (highlighted in pink color in Figure 2(a)) have decreased compared to those of the pristine MoS_2 (18−15% to 13−10% respectively). This can be explained by the partial saturation of these vacancies with hydrogen atoms forming Mo−H bonds. These Sv peaks completely disappear after the second dose and all core levels BE are shifted by −0.3 eV, indicating a complete saturation of the Sv. In this case both, the Mo 3d and S 2p peaks became sharper (fwhm = 0.6 to 0.5 eV). The saturation of these vacancies gradually reduced the n-type doping of the MoS_2 decreasing the distance of the VBM to the Fermi level (FL) as shown in Figure 3(a) and (b), from 1.25 eV for the

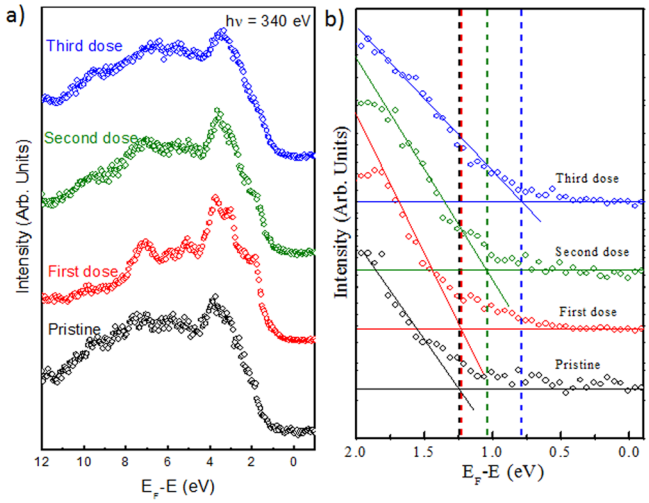


Figure 3. (a) Valence band intensity integrated spectra as a function of the binding energy of pristine MoS_2 and hydrogenated MoS_2 (for three doses). (b) Zoom of (a). The experimental data points are displayed as dots.

pristine MoS_2 to 1.05 eV (almost midgap, considering a quasi-particle bandgap of 2 eV[38]) for the second hydrogen dose. We notice that the spectra in Figure 3(a) show similar characteristic peaks, before and after hydrogenation (for different doses), that are related to MoS_2 valence band.[39] The shifts of hydrogenated MoS_2 shown in Figure 3(b) are caused by the rigid energy shift of all core-levels. When the hydrogen dose is further increased the core level peaks still shift toward lower binding energy (−0.5 eV), which correspond to a distance of the VBM to the FL of about 0.75 eV. This means that a p-type doping is now induced in the MoS_2 flakes. This huge hydrogen dose (∼8 × 10^4 L) probably starts to induce new Sv, directly replaced by hydrogen forming Mo−H bonds.[40−42] The formations of Mo−H bonds and the saturation of the Sv replace the donor gap state present in the pristine MoS_2 to new acceptor gap state related to the Mo−H bond formation as shown below by DFT calculations. Moreover, the Mo 3d and S 2p spectra show also the presence of a new component at lower binding energy with respect to the main doublet peaks (∼0.8 eV). These components are probably related to the formation of the

DOI: 10.1021/acsnano.6b07661
ACS Nano 2017, 11, 1755−1761

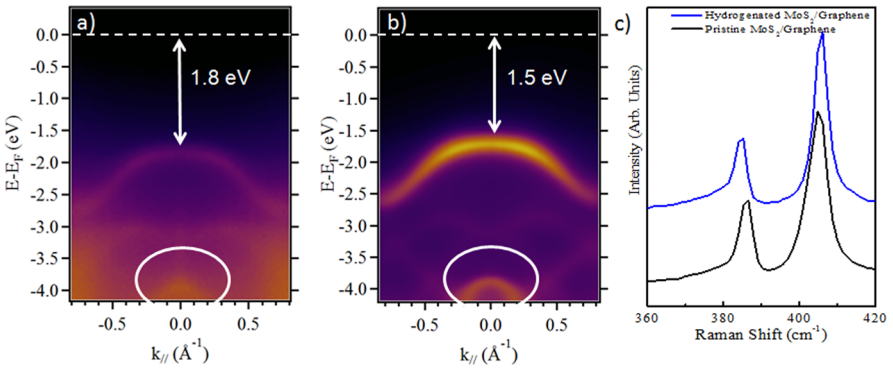


Figure 4. (a,b) ARPES measurements at room temperature of pristine MoS_2/graphene at $h\nu$ = 50 eV and hydrogenated MoS_2/graphene heterostructure at $h\nu$ = 100 eV, respectively along the graphene ΓK direction. The Fermi level position is located at the zero of the binding energy (marked as a white dashed line), the white circles highlight the shift in the position of the band located at around −4 eV. (c) Comparison between the Raman spectra of MoS_2 before (in black line) and after (in blue line) hydrogenation.

octahedral 1T phase of MoS_2 induced by the high density of hydrogen atoms present in the sample.

The electronic structure and the stability of the hydrogenated MoS_2, kept one month under ambient conditions after the hydrogenation (a dose of 5 × 10^3 L), were studied using ARPES (Figure 4). Figures 4(a) and (b) show the ARPES momentum energy image, before and after hydrogenation respectively, around the Γ point of the Brillouin zone (BZ). The expected signal of the monolayer MoS_2 valence band is visible.[43,44] The shape of the upper band of the valence bands is not modified but only shifted toward the FL because of the exposure to the hydrogen atoms. Moreover, we notice the same shift for the other bands around −3 eV and −4 eV (highlighted by the white circles). Hence, we can claim that the hydrogenation induces a uniform shift of all the bands forming the valence bandstructure of MoS_2. The sharp and intense experimental band structure of Figure 4(b) confirms the hydrogenation process preserves the high structural quality of the MoS_2 flakes. The ARPES quality is even better after hydrogenation suggesting that the hydrogen treatment improves the surface quality of the MoS_2 by passivating the Sv.

ARPES measurement, perpendicular to the Γ−K direction of the p-doped graphene underlayer BZ before and after the hydrogenation of MoS_2/p-doped graphene underlayer, are shown in the Supporting Information in Figure S2. In this intensity map, the graphene underlayer presents two π bands, which is the clear signature of the interlayer decoupling induced by the hydrogenation of the epitaxial graphene giving rise to a quasi-free-standing bilayer graphene and a completely saturated SiC surface. Moreover, in this sample orientation, the two branches of the graphene π bands can be observed[45] allowing the determination of the Dirac point position with respect to the FL. Close inspection of the dispersion relation around K reveals that the FL is located at 0.25 eV below the Dirac points for the pristine MoS_2/graphene heterostructure and is not modified after the hydrogen dose. This value corresponds to a hole doping level of the graphene underlayer of about 3.8 × 10^{12} cm^{-2}.

In order to probe the effects of atomic hydrogen on the electronic properties of hydrogen doped MoS_2 (8 × 10^4 L), we performed micro-Raman spectroscopy on two flakes with the same orientation angle with respect to the graphene underlying substrate. This choice is made so that we can assume that the flakes are subjected to the same orientation-induced strain.[38,46,47] In Figure 4(c), the Raman spectra of MoS_2 before and after the hydrogenation are shown. The two vibrational modes are separated by about 19 cm^{-1} which corresponds to a single layered MoS_2 as was reported for MoS_2 monolayer.[48,49] After the treatment, we clearly observe that a downshift of the E^1_{2g} peak has occurred together with a splitting of this peak. This is likely due to a strain induced by the hydrogen intercalation (which is probably responsible for the appearance of the 1T-phase);[50] this strain is tensile as indicated by the direction of the E^1_{2g} shift.[47,51−53] The peak splitting gave rise to two distinctive E^1_{2g} modes, similarly to what was observed by A. Azcatl *et al.*, who doped the MoS_2 using nitrogen plasma.[21] Furthermore, the A_{1g} peak is slightly upshifted which can be explained by a change of the doping level in MoS_2,[38,54] *i.e.*, the saturation of the Sv, the hydrogen atoms introduction, and eventually the removal of S atoms.[14,55] On the other hand, the increase of the A_{1g} peak intensity or in other words the increase of the ratio of intensities A_{1g}/E^1_{2g} is consistent with what was reported on the p doping of MoS_2.[20] According to these Raman results, we show that the hydrogenation of MoS_2 was successfully done leading to a nondefective MoS_2. Photoluminescence (PL) spectra of pristine and hydrogenated MoS_2 are provided in Figure S3. We notice that the PL intensity decreases after hydrogenation; this PL quenching can be explained by the suppression of defects from MoS_2 at room temperature as was observed for pristine and irradiated MoS_2.[14] This confirms again that the used process is noninvasive and that it is possible to hydrogenate MoS_2 even with better quality.

In order to gain insights into this doping change from n to p of the MoS_2 flakes we performed first principle calculations based on DFT. Figure 5 shows the total density of state (DOS) of a perfect MoS_2 monolayer (black curve), MoS_2 with Sv (red curve) and Sv saturated by hydrogen atoms (blue curve). As expected, the presence of Sv induces defect state in the gap, located at about 0.75 eV below the conduction band minimum (CBM). This donor state is in fact responsible for the intrinsic n-type doping of the pristine MoS_2 flake as measured by XPS. Our calculation shows that Mo−H bonds induce new gap state at about 0.16 eV above the valence band maximum (VBM). The presence of this acceptor like state confirms the p-type behavior observed experimentally after the MoS_2 hydrogenation. The combination of XPS experiments and DFT gives a global picture of the structural and electronic MoS_2 properties after the hydrogenation process. A single layer MoS_2 includes well-known Sv as displayed in Figure 6(a). After the first hydrogenation (Figure 6(b)), the hydrogen atoms react

DOI: 10.1021/acsnano.6b07661
ACS Nano 2017, 11, 1755−1761

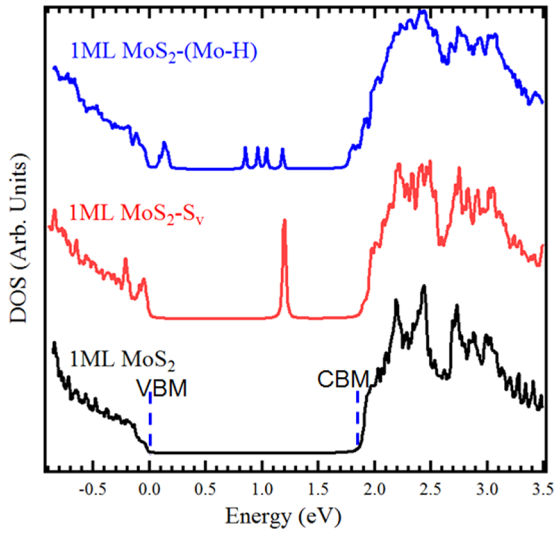


Figure 5. Total DOS of pristine MoS_2 (black line), MoS_2 with Sv (red line), and hydrogenated MoS_2 (blue line) using DFT calculations.

with the unbound Mo atoms. This model explains the elimination of defect peaks in Mo 3d. At high atomic hydrogen dose, if new Sv vacancies are created by high hydrogen dose, they are readily replaced by the hydrogen atoms increasing the p-type doping of the MoS_2 as indicated by the energy shift of the Mo-3d and S-2p core level spectra toward lower binding energy and the reduction of the energy distance of the VBM with respect to the FL upon hydrogenation (Figure 6(c)).

CONCLUSIONS

In summary, we conducted a comprehensive study of the interaction of atomic hydrogen with monolayer MoS_2. The pristine MoS_2 has sulfur vacancies, which are responsible for its intrinsic n-type doping. During hydrogen dosing, the hydrogen atoms react with the under-coordinated Mo atoms filling the Sv. When all the vacancies are filled, the MoS_2 becomes almost intrinsic (VBM = 1.05 eV). At higher atomic hydrogenation, the hydrogen breaks the Mo−S bonds and passivates the newly created vacancies inducing a p-type doping in the MoS_2 sample. This model suggested by the HR-XPS results is corroborated by DFT calculations predicting the presence of an acceptor gap state upon the formation of the Mo−H bonds. As Raman and ARPES measurements show that the hydrogen dosing process does not alter the quality of the MoS_2 flakes since it preserves a well-defined electronic structure. Therefore, we see this hydrogenation process as an efficient method to reduce the defects in MoS_2 flakes, control, and switch from n to p the intrinsic as-grown doping. Such control of doping in 2D TMDs is of great importance for potential nanoscale, flexible devices applications based on these materials.

METHODS

Bilayer Graphene on SiC(0001). Bilayer graphene was produced by thermal heating the SiC(0001) substrate. Before the graphitization, the substrate was etched with hydrogen (100% H_2) at 1550 °C to produce well-ordered atomic terraces of SiC. The substrate was heated to 1000 °C and then further heated at 1550 °C under argon (800 mbar).

Growth and Transfer of MoS_2. Large scale MoS_2 monolayer flakes (≈20 to ≈100 μm) have been grown by Chemical Vapor Deposition (CVD) on oxidized silicon substrate (see ref 56). The MoS_2 flakes transferred onto the graphene retain their triangular shapes with unchanged lateral sizes. Before any measurement, the MoS_2 sample was annealed at 300 °C for 30 min in ultrahigh vacuum ($P \approx 10^{-10}$ mbar), in order to remove the residual surface contaminations induced by the wet transfer.

Atomic Hydrogen Doping. The hydrogenation process has been performed at room temperature under a pressure of 2×10^{-5} mbar of H_2 in order to avoid hydrogen etching of the MoS_2 layer. The hydrogenation process lasted 3 h, under a lower pressure of H_2, in order to control the phenomena that may occur on the MoS_2 properties. This procedure has been repeated twice, after each the sample was fully characterized by means of XPS measurements.

HR-XPS. HR-XPS experiments were carried out on the TEMPO beamline[57] (SOLEIL French synchrotron facility) at room temperature. The photon source was a HU80 Apple II undulator set to deliver horizontally linearly polarized light. The photon energy was selected using a high-resolution plane grating monochromator, with a resolving power $E/\Delta E$ that can reach 15 000 on the whole energy range (45−1500 eV). During the XPS measurements, the photoelectrons were detected at 0° from the sample surface normal $\vec{n}$ and at 46° from the polarization vector $\vec{E}$. The spot size was 80 × 40 (H × V) μm^2.

A Shirley background was subtracted in all core level spectra. The C 1s spectrum was fitted by a sum of a Gaussian function convoluted with a Doniach-Sunjic line shape. An asymmetry factor α was used, where α = 0.1 eV (G peak) and α = 0 eV (SiC). The Mo 3d and S 2p spectra were fitted by sums of Voigt curves, *i.e.*, the convolution of a

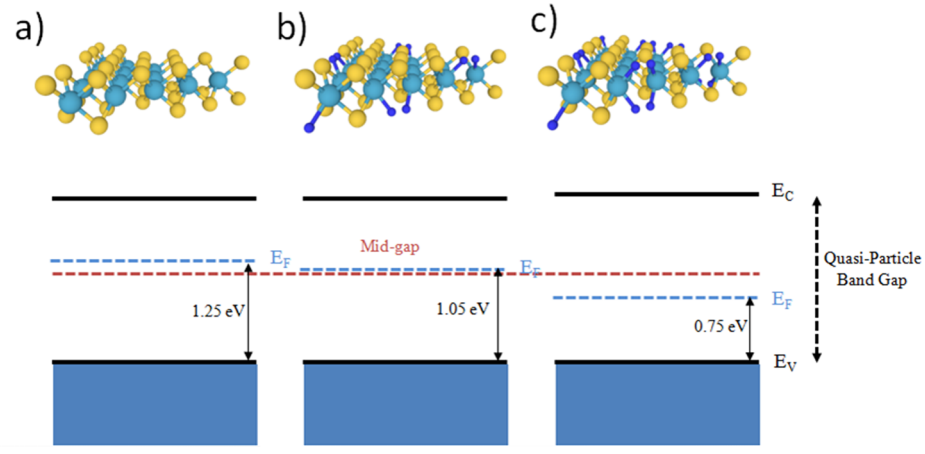


Figure 6. Band diagram showing the evolution of MoS_2 Fermi level (a) before hydrogenation, (b) upon the first exposure to hydrogen, and (c) after the complete hydrogenation.

DOI: 10.1021/acsnano.6b07661
ACS Nano 2017, 11, 1755−1761

Gaussian (of full-width at half-maximum GW) by a Lorentzian (of full-width at half-maximum LW). The LW was fixed at 90 meV for Mo 3d and S 2p.[32]

Angle-Resolved Photoemission Spectroscopy. The ARPES measurements were conducted at the CASSIOPEE beamline of Synchrotron SOLEIL (Saint-Aubin, France). We used horizontally linearly polarized photons of 50 eV and a hemispherical electron analyzer with vertical slits to allow band mapping. The total angle and energy resolutions were 0.25° and 25 meV. The mean diameter of the incident photon beam was smaller than 50 μm. All ARPES experiments were done at room temperature.

DFT Calculations. First-principles calculations have been performed using a very efficient DFT localized orbital molecular dynamic technique (FIREBALL).[58,59] Basis sets of sp3d5 for S and Mo were used with cutoff radii (in atomic units) s = 3.9, p = 4.5, d = 5.0 (S) and s = 5.0, p = 4.5, d = 4.8 (Mo).[47] In this study we have considered a standard (5 × 5) unit cell of MoS_2 that has been optimized as a pristine, with an S vacancy and with an H-filled S vacancy, before calculating the corresponding DOS.

ASSOCIATED CONTENT

Supporting Information

The Supporting Information is available free of charge on the ACS Publications website at DOI: 10.1021/acsnano.6b07661.

Figures S1−S3 (PDF)

AUTHOR INFORMATION

Corresponding Author

*E-mail: abdelkarim.ouerghi@lpn.cnrs.fr.

ORCID

Abdelkarim Ouerghi: 0000-0002-1898-2765

Notes

The authors declare no competing financial interest.

ACKNOWLEDGMENTS

This work was supported by the ANR H2DH grants. C.H.N. and A.T.C.J. acknowledge support from the National Science Foundation EFRI-2DARE program, grant number ENG-1542879.

REFERENCES

(1) Furchi, M. M.; Polyushkin, D. K.; Pospischil, A.; Mueller, T. Mechanisms of Photoconductivity in Atomically Thin MoS2. *Nano Lett.* **2014**, *14* (11), 6165−6170.

(2) Buscema, M.; Island, J. O.; Groenendijk, D. J.; Blanter, S. I.; Steele, G. a; van der Zant, H. S. J.; Castellanos-Gomez, A. Photocurrent Generation with Two-Dimensional van Der Waals Semiconductors. *Chem. Soc. Rev.* **2015**, *44* (11), 3691−3718.

(3) Lopez-Sanchez, O.; Lembke, D.; Kayci, M.; Radenovic, A.; Kis, A. Ultrasensitive Photodetectors Based on Monolayer MoS2. *Nat. Nanotechnol.* **2013**, *8* (7), 497−501.

(4) Splendiani, A.; Sun, L.; Zhang, Y.; Li, T.; Kim, J.; Chim, C. Y.; Galli, G.; Wang, F. Emerging Photoluminescence in Monolayer MoS2. *Nano Lett.* **2010**, *10* (4), 1271−1275.

(5) Conley, H. J.; Wang, B.; Ziegler, J. I.; Haglund, R. F.; Pantelides, S. T.; Bolotin, K. I. Bandgap Engineering of Strained Monolayer and Bilayer MoS 2. *Nano Lett.* **2013**, *13* (8), 3626−3630.

(6) Li, Y.; Tongay, S.; Yue, Q.; Kang, J.; Wu, J.; Li, J. Metal to Semiconductor Transition in Metallic Transition Metal Dichalcogenides. *J. Appl. Phys.* **2013**, *114*, 174307.

(7) Tang, Q.; Jiang, D. Stabilization and Band-Gap Tuning of the 1T-MoS 2 Monolayer by Covalent Functionalization. *Chem. Mater.* **2015**, *27*, 3743−3748.

(8) Pierucci, D.; Sediri, H.; Hajlaoui, M.; Velez-fort, E.; Dappe, Y. J.; Silly, M. G.; Belkhou, R.; Shukla, A.; Sirotti, F.; Gogneau, N.; Ouerghi, A. Self-Organized Metal − Semiconductor Epitaxial Graphene Layer on off-Axis 4H-SiC (0001). *Nano Res.* **2015**, *8* (3), 1026−1037.

(9) Li, Y.; Duerloo, K.-A. N.; Wauson, K.; Reed, E. J. Structural Semiconductor-to-Semimetal Phase Transition in Two-Dimensional Materials Induced by Electrostatic Gating. *Nat. Commun.* **2016**, *7*, 10671.

(10) Krivosheeva, A. V.; Shaposhnikov, V. L.; Borisenko, V. E.; Lazzari, J. Theoretical Study of Defect Impact on Two-Dimensional MoS 2. *J. Semicond.* **2015**, *36* (12), 122002.

(11) Lin, Z.; Carvalho, B. R.; Kahn, E.; Lv, R.; Rao, R.; Terrones, H. Defect Engineering of Two-Dimensional Transition Metal Dichalcogenides. *2D Mater.* **2016**, *3*, 22002.

(12) Zhou, W.; Zou, X.; Najmaei, S.; Liu, Z.; Shi, Y.; Kong, J.; Lou, J. Intrinsic Structural Defects in Monolayer Molybdenum Disul Fi de. *Nano Lett.* **2013**, *13* (6), 2615−2622.

(13) Liu, D.; Guo, Y.; Fang, L.; Robertson, J.; Liu, D.; Guo, Y.; Fang, L.; Robertson, J. Sulfur Vacancies in Monolayer MoS2 and Its Electrical Contacts. *Appl. Phys. Lett.* **2013**, *103*, 183113.

(14) Parkin, W. M.; Balan, A.; Liang, L.; Das, P. M.; Lamparski, M.; Carl, H.; Rodríguez-manzo, J. A.; Johnson, A. T. C.; Meunier, V.; Drndic, M. Raman Shifts in Electron-Irradiated Monolayer MoS 2. *ACS Nano* **2016**, *10* (4), 4134−4142.

(15) Addou, R.; Mcdonnell, S.; Barrera, D.; Guo, Z.; Azcatl, A.; Wang, J.; Zhu, H.; Hinkle, C. L.; Quevedo-lopez, M.; Alshareef, H. N.; Colombo, L.; Hsu, J. W. P.; Wallace, R. M. Impurities and Electronic Property Variations of Natural MoS 2 Crystal Surfaces. *ACS Nano* **2015**, *9*, 9124−9133.

(16) González, C.; Biel, B.; Dappe, Y. J. Theoretical Characterisation of Point Defects on a MoS2Monolayer by Scanning Tunnelling Microscopy. *Nanotechnology* **2016**, *27*, 105702.

(17) Guo, Y.; Liu, D.; Robertson, J. Chalcogen Vacancies in Monolayer Transition Metal Dichalcogenides and Fermi Level Pinning at Contacts. *Appl. Phys. Lett.* **2015**, *106* (17), 48−53.

(18) Nan, H.; Wang, Z.; Wang, W.; Liang, Z.; Lu, Y.; Chen, Q.; He, D.; Tan, P.; Miao, F.; Wang, X.; Wang, J.; Ni, Z. Strong Photoluminescence Enhancement of MoS2 through Defect Engineering and Oxygen Bonding. *ACS Nano* **2014**, *8* (6), 5738−5745.

(19) Qin, S.; Lei, W.; Liu, D.; Chen, Y. In-Situ and Tunable Nitrogen-Doping of MoS 2 Nanosheets. *Sci. Rep.* **2014**, *4*, 7582.

(20) Laskar, M. R.; Nath, D. N.; Ma, L.; Ii, E. W. L.; Lee, C. H.; Kent, T.; Yang, Z.; Mishra, R.; Roldan, M. A.; Idrobo, J.; Pantelides, S. T.; Pennycook, S. J.; Myers, C.; Wu, Y.; Rajan, S.; Idrobo, J.; Pantelides, S. T.; Pennycook, S. J. P-Type Doping of MoS2 Thin Films Using Nb. *Appl. Phys. Lett.* **2014**, *92104*, 104−108.

(21) Azcatl, A.; Qin, X.; Prakash, A.; Zhang, C.; Cheng, L.; Wang, Q.; Lu, N.; Kim, M. J.; Kim, J.; Cho, K.; Hinkle, C. L.; Appenzeller, J.; Wallace, R. M. Covalent Nitrogen Doping and Compressive Strain in MoS 2 by Remote N 2 Plasma Exposure. *Nano Lett.* **2016**, *16* (9), 5437−5443.

(22) Pallecchi, E.; Lafont, F.; Cavaliere, V.; Schopfer, F.; Mailly, D.; Poirier, W.; Ouerghi, A. High Electron Mobility in Epitaxial Graphene on 4H-SiC(0001) *via* Post-Growth Annealing under Hydrogen. *Sci. Rep.* **2014**, *4*, 4558.

(23) Robinson, J. A.; Hollander, M.; Labella, M.; Trumbull, K. A.; Cavalero, R.; Snyder, D. W. Epitaxial Graphene Transistors: Enhancing Performance *via* Hydrogen. *Nano Lett.* **2011**, *11*, 3875−3880.

(24) Henck, H.; Pierucci, D.; Ben Aziza, Z.; Silly, M. G.; Gil, B.; Sirotti, F.; Cassabois, G.; Ouerghi, A. Stacking Fault and Defects in Single Domain Multilayered Hexagonal Boron Nitride. *Appl. Phys. Lett.* **2017**, *110* (2), 23101.

(25) Yan, L.; Zheng, B.; Zhao, F.; Li, S.; Gao, X.; Xu, B.; Weiss, S.; Zhao, Y. Chem Soc Rev Chemistry and Physics of a Single Atomic Layer: Strategies and Challenges for Functionalization of Graphene and Graphene-Based Materials. *Chem. Soc. Rev.* **2012**, *41*, 97−114.

(26) Pallecchi, E.; Ridene, M.; Kazazis, D.; Mathieu, C.; Schopfer, F.; Poirier, W.; Mailly, D.; Ouerghi, A. Observation of the Quantum Hall Effect in Epitaxial Graphene on SiC(0001) with Oxygen Adsorption. *Appl. Phys. Lett.* **2012**, *100* (25), 253109.

(27) Pallecchi, E.; Ridene, M.; Kazazis, D.; Lafont, F.; Schopfer, F.; Poirier, W.; Goerbig, M. O.; Mailly, D.; Ouerghi, A. Insulating to Relativistic Quantum Hall Transition in Disordered Graphene. *Sci. Rep* **2013**, *3*, 1791.
(28) Riedl, C.; Coletti, C.; Iwasaki, T.; Zakharov, a. a.; Starke, U. Quasi-Free-Standing Epitaxial Graphene on SiC Obtained by Hydrogen Intercalation. *Phys. Rev. Lett.* **2009**, *103* (24), 246804.
(29) Henck, H.; Pierucci, D.; Chaste, J.; Naylor, C. H.; Avila, J.; Balan, A.; Silly, M. G.; Maria, C.; Sirotti, F.; Johnson, A. T. C.; Lhuillier, E.; Ouerghi, A. Electrolytic Phototransistor Based on Graphene-MoS2 van Der Waals P-N Heterojunction with Tunable Photoresponse P-N Heterojunction with Tunable Photoresponse. *Appl. Phys. Lett.* **2016**, *109*, 113103.
(30) Pierucci, D.; Henck, H.; Avila, J.; Balan, A.; Naylor, C. H.; Patriarche, G.; Dappe, Y. J.; Silly, M. G.; Sirotti, F.; Johnson, A. T. C.; Asensio, M. C.; Ouerghi, A. Band Alignment and Minigaps in Monolayer MoS2-Graphene van Der Waals Heterostructures. *Nano Lett.* **2016**, *16* (7), 4054−4061.
(31) Boukhicha, M.; Calandra, M.; Measson, M. A.; Lancry, O.; Shukla, A. Anharmonic Phonons in Few-Layer MoS2: Raman Spectroscopy of Ultralow Energy Compression and Shear Modes. *Phys. Rev. B: Condens. Matter Mater. Phys.* **2013**, *87*, 195316.
(32) Mattila, S.; Leiro, J. a.; Heinonen, M.; Laiho, T. Core Level Spectroscopy of MoS2. *Surf. Sci.* **2006**, *600* (24), 5168−5175.
(33) Kim, I. S.; Sangwan, V. K.; Jariwala, D.; Wood, J. D.; Park, S.; Chen, K.; Shi, F.; Ruiz-zepeda, F.; Ponce, A.; Jose, M.; Dravid, V. P.; Marks, T. J.; Hersam, M. C.; Lincoln, J. Influence of Stoichiometry on the Optical and Electrical Properties of Chemical Vapor Deposition Derived MoS 2. *ACS Nano* **2014**, *8* (10), 10551−10558.
(34) Eda, G.; Yamaguchi, H.; Voiry, D.; Fujita, T.; Chen, M.; Chhowalla, M. Photoluminescence from Chemically Exfoliated MoS2. *Nano Lett.* **2011**, *11* (12), 5111−5116.
(35) Levasseur, a; Vinatier, P.; Gonbeau, D. X-Ray Photoelectron Spectroscopy: A Powerful Tool for a Better Characterization of Thin Film Materials. *Bull. Mater. Sci.* **1999**, *22* (3), 607−614.
(36) Baker, M. A.; Gilmore, R.; Lenardi, C.; Gissler, W. XPS Investigation of Preferential Sputtering of S from MoS 2 and Determination of MoS X Stoichiometry from Mo and S Peak Positions. *Appl. Surf. Sci.* **1999**, *150*, 255−262.
(37) Fleischauer, P. D.; Lince, J. R. A Comparison of Oxidation and Oxygen Substitution in MoS 2 Solid Film Lubricants. *Tribol. Int.* **1999**, *32*, 627−636.
(38) Liu, X.; Balla, I.; Bergeron, H.; Campbell, G. P.; Bedzyk, M. J.; Hersam, M. C. Rotationally Commensurate Growth of MoS2 on Epitaxial Graphene. *ACS Nano* **2015**, *10* (1), 1067−1075.
(39) Han, S. W.; Cha, G. B.; Frantzeskakis, E.; Razado-Colambo, I.; Avila, J.; Park, Y. S.; Kim, D.; Hwang, J.; Kang, J. S.; Ryu, S.; Yun, W. S.; Hong, S. C.; Asensio, M. C. Band-Gap Expansion in the Surface-Localized Electronic Structure of MoS 2(0002). *Phys. Rev. B: Condens. Matter Mater. Phys.* **2012**, *86*, 115105.
(40) Search, H.; Journals, C.; Contact, A.; Iopscience, M.; Phys, S. S.; Address, I. P. The Vibration Spectrum of Hydrogen Bound by Molybdenum Sulphide Catalysts. *J. Phys. C: Solid State Phys.* **1981**, *14*, 4969−4983.
(41) Cristol, S.; Paul, J. F.; Payen, E.; Hutschka, F. Theoretical Study of the MoS 2 (100) Surface: A Chemical Potential Analysis of Sulfur and Hydrogen Coverage. *J. Phys. Chem. B* **2000**, *104*, 11220−11229.
(42) Spirko, J. A.; Neiman, M. L.; Oelker, A. M.; Klier, K. Electronic Structure and Reactivity of Defect MoS 2 II. Bonding and Activation of Hydrogen on Surface Defect Sites and Clusters. *Surf. Sci.* **2004**, *572*, 191−205.
(43) Coy Diaz, H.; Avila, J.; Chen, C.; Addou, R.; Asensio, M. C.; Batzill, M. Direct Observation of Interlayer Hybridization and Dirac Relativistic Carriers in Graphene/MoS2 van Der Waals Heterostructures. *Nano Lett.* **2015**, *15* (2), 1135−1140.
(44) Pierucci, D.; Henck, H.; Naylor, C. H.; Sediri, H.; Lhuillier, E.; Balan, A.; Rault, J. E.; Dappe, Y. J.; Bertran, F.; Le Févre, P.; Johnson, A. T. C.; Ouerghi, A. Large Area Molybdenum Disulphide-Epitaxial Graphene Vertical Van Der Waals Heterostructures. *Sci. Rep.* **2016**, *6*, 26656.
(45) Gierz, I.; Henk, J.; Hochst, H.; Ast, C. R.; Kern, K. Illuminating the Dark Corridor in Graphene: Polarization Dependence of Angle-Resolved Photoemission Spectroscopy on Graphene. *Phys. Rev. B: Condens. Matter Mater. Phys.* **2011**, *83* (12), 1−4.
(46) Wang, Z.; Chen, Q.; Wang, J. Electronic Structure of Twisted Bilayers of graphene/MoS2 and MoS2/MoS2. *J. Phys. Chem. C* **2015**, *119* (9), 4752−4758.
(47) Ben Aziza, Z.; Henck, H.; Di, D.; Pierucci, D.; Chaste, J.; Naylor, C. H.; Balan, A.; Dappe, Y. J.; Johnson, A. T. C.; Ouerghi, A. Bandgap Inhomogeneity of MoS 2 Monolayer on Epitaxial Graphene Bilayer in van Der Waals P-N Junction. *Carbon* **2016**, *110*, 396−403.
(48) Li, H.; Zhang, Q.; Yap, C. C. R.; Tay, B. K.; Edwin, T. H. T.; Olivier, A.; Baillargeat, D. From Bulk to Monolayer MoS 2: Evolution of Raman Scattering. *Adv. Funct. Mater.* **2012**, *22* (7), 1385−1390.
(49) Lee, C.; Yan, H.; Brus, L. E.; Heinz, T. F.; Hone, Ḱ. J.; Ryu, S. Anomalous Lattice Vibrations of Single-and Few-Layer MoS2. *ACS Nano* **2010**, *4* (5), 2695−2700.
(50) Han, S. W.; Yun, W. S.; Lee, J. D.; Hwang, Y. H.; Baik, J.; Shin, H. J.; Lee, W. G.; Park, Y. S.; Kim, K. S. Hydrogenation-Induced Atomic Stripes on the 2 H -MoS 2 Surface. *Phys. Rev. B: Condens. Matter Mater. Phys.* **2015**, *241303*, 1−5.
(51) Wang, Y.; Cong, C.; Qiu, C.; Yu, T. Raman Spectroscopy Study of Lattice Vibration and Crystallographic Orientation of Monolayer mos2 under Uniaxial Strain. *Small* **2013**, *9* (17), 2857−2861.
(52) Hui, Y. Y.; Liu, X.; Jie, W.; Chan, N. Y.; Hao, J.; Hsu, Y. T.; Li, L. J.; Guo, W.; Lau, S. P. Exceptional Tunability of Band Energy in a Compressively Strained Trilayer. *ACS Nano* **2013**, *7* (8), 7126−7131.
(53) Nayak, A. P.; Bhattacharyya, S.; Zhu, J.; Liu, J.; Wu, X.; Pandey, T.; Jin, C.; Singh, A. K.; Akinwande, D.; Lin, J. Pressure-induced semiconducting to metallic Transition in Multilayered Molybdenum Disulphide. *Nat. Commun.* **2014**, *5*, 3731.
(54) Chakraborty, B.; Bera, A.; Muthu, D. V. S.; Bhowmick, S.; Waghmare, U. V.; Sood, A. K. Symmetry-Dependent Phonon Renormalization in Monolayer MoS 2 Transistor. *Phys. Rev. B: Condens. Matter Mater. Phys.* **2012**, *85* (16), 2−5.
(55) Kim, B. H.; Park, M.; Lee, M.; Baek, S. J.; Jeong, H. Y.; Choi, M.; Chang, S. J.; Hong, W. G.; Kim, T. K.; Moon, H. R.; Park, W.; Park, N.; Jun, Y. RSC Advances Structure of MoS2 Induced by Molecular Hydrogen Treatment at Room Temperature. *RSC Adv.* **2013**, *3*, 18424−18429.
(56) Han, G. H.; Kybert, N. J.; Naylor, C. H.; Lee, B. S.; Ping, J.; Park, J. H.; Kang, J.; Lee, S. Y.; Lee, Y. H.; Agarwal, R.; Johnson, a T. C. Seeded Growth of Highly Crystalline Molybdenum Disulphide Monolayers at Controlled Locations. *Nat. Commun.* **2015**, *6*, 6128.
(57) Polack, F.; Silly, M.; Chauvet, C.; Lagarde, B.; Bergeard, N.; Izquierdo, M.; Chubar, O.; Krizmancic, D.; Ribbens, M.; Duval, J.-P.; Basset, C.; Kubsky, S.; Sirotti, F.; Garrett, R.; Gentle, I.; Nugent, K.; Wilkins, S. TEMPO: A New Insertion Device Beamline at SOLEIL for Time Resolved Photoelectron Spectroscopy Experiments on Solids and Interfaces. *AIP Conf. Proc.* **2009**, *1234* (2010), 185−188.
(58) Lewis, J. P.; Jelínek, P.; Ortega, J.; Demkov, A. A.; Trabada, D. G.; Haycock, B.; Wang, H.; Adams, G.; Tomfohr, J. K.; Abad, E.; Wang, H.; Drabold, D. A. Advances and Applications in the FIREBALL Ab Initio Tight-Binding Molecular-Dynamics Formalism. *Phys. Status Solidi Basic Res.* **2011**, *248* (9), 1989−2007.
(59) Jelínek, P.; Wang, H.; Lewis, J.; Sankey, O.; Ortega, J. Multicenter Approach to the Exchange-Correlation Interactions in Ab Initio Tight-Binding Methods. *Phys. Rev. B: Condens. Matter Mater. Phys.* **2005**, *71*, 235101.

DOI: 10.1021/acsnano.6b07661
ACS Nano 2017, 11, 1755−1761